

Document downloaded from:

<http://hdl.handle.net/10251/38674>

This paper must be cited as:

Santamaría Pérez, D.; Bandiello, E.; Errandonea, D.; Ruiz-Fuertes, J.; Gómis Hilario, O.; Sans, J.Á.; Manjón, FJ; Rodríguez-Hernández, P.; Muñoz, A. (2013). Phase behaviour of Ag₂CrO₄ under compression: Structural, vibrational, and optical properties. *Journal of Physical Chemistry C*. 117:12239-12248. doi:10.1021/jp401524s.



The final publication is available at

<http://dx.doi.org/10.1021/jp401524s>

Copyright American Chemical Society

Phase Behaviour of Ag₂CrO₄ under Compression: Structural, Vibrational, and Optical Properties

Journal:	<i>The Journal of Physical Chemistry</i>
Manuscript ID:	jp-2013-01524s
Manuscript Type:	Article
Date Submitted by the Author:	12-Feb-2013
Complete List of Authors:	Santamaría-Pérez, David; Universidad Complutense de Madrid, Química Física I; Universitat de Valencia, Departamento de Fisica Aplicada Bandiello, Enrico; Universitat de Valencia, Departamento de Fisica Aplicada Errandonea, Daniel; Universitat de Valencia, Departamento de Fisica Aplicada Ruiz-Fuertes, Javier; University of Valencia, Gomis, Oscar; Universitat Politecnica de Valecia, Centro de Tecnologias Fisicas Sans, Juan Angel; Universidad Politecnica de Valencia, Applied Physics Manjon, Francisco J.; Universidad Politecnica de Valencia, Applied Physics Rodriguez-Hernandez, Placida; Universidad de la Laguna, Muñoz, A.; Universidad de la Laguna,

SCHOLARONE™
Manuscripts

1
2
3 **Phase behaviour of Ag_2CrO_4 under compression:**
4
5
6
7 **Structural, vibrational, and optical properties.**
8
9

10
11
12 *David Santamaría-Pérez^{1,2,*}, Enrico Bandiello¹, Daniel Errandonea¹, Javier Ruiz-Fuertes^{1,3},*

13
14
15 *Oscar Gomis⁴, Juan Angel Sans⁵, Francisco Javier Manjón⁵, Plácida Rodríguez-Hernández⁶,*

16
17
18 *Alfonso Muñoz⁶.*

19
20
21
22 ¹ Departamento de Física Aplicada-ICMUV, MALTA Consolider Team, Universidad de
23
24 Valencia, C/Dr. Moliner 50, Burjassot, 46100 Valencia, Spain

25
26 ² Departamento de Química Física I, Universidad Complutense de Madrid, MALTA
27
28 Consolider Team, Avenida Complutense s/n, 28040 Madrid, Spain

29
30 ³ Lyman Laboratory of Physics, Harvard University, Cambridge, MA 02138, USA

31
32
33 ⁴ Centro de Tecnologías Físicas: Acústica, Materiales y Astrofísica, MALTA Consolider
34
35 Team, Universitat Politècnica de València, 46022 València, Spain

36
37 ⁵ Instituto de Diseño para la Fabricación y Producción Automatizada, MALTA
38
39 Consolider Team, Universitat Politècnica de València, 46022 València, Spain

40
41
42 ⁶ Departamento de Física Fundamental II, Instituto de Materiales y Nanotecnología,
43
44 MALTA Consolider Team, Universidad de La Laguna, 38205 Tenerife, Spain
45
46
47
48
49
50
51
52
53
54
55
56
57
58
59
60

1
2
3
4
5 **Abstract.-** We have performed an experimental study of the crystal structure, lattice
6 dynamics, and optical properties of silver chromate (Ag_2CrO_4) at ambient temperature
7 and high pressures. In particular, the crystal structure, Raman-active phonons, and
8 electronic band gap have been accurately determined. When the initial orthorhombic
9 *Pnma* Ag_2CrO_4 structure (Phase I) is squeezed up to ~ 4 GPa, a previously undetected
10 phase (Phase II) has been observed with a 0.95% volume collapse. The structure of
11 Phase II can be indexed into a similar orthorhombic cell as Phase I, and the transition
12 can be considered as an isostructural transition. This collapse is mainly due to the
13 drastic contraction of the *a* axis ($\sim 1.3\%$). A second phase transition to Phase III occurs
14 at ~ 13 GPa, to a structure not yet determined. First-principles calculations have been
15 unable to reproduce the isostructural phase transition likely due to electronic
16 considerations in chromium atoms. Calculations propose the stabilization of a spinel-
17 type structure at 11 GPa. This phase is not detected in experiments probably due to the
18 presence of kinetic barriers.
19
20
21
22
23
24
25
26
27
28
29
30
31
32
33
34
35
36
37
38
39
40

41 **Pacs Numbers:** 62.50.+p, 71.20.Nr

42
43 **Keywords:** silver chromate, high pressure, phase transitions, crystal structure, Raman
44 spectroscopy, optical absorption
45
46
47
48
49
50
51
52
53
54

55
56
57 * Corresponding author, Email: dsantamaria@quim.ucm.es, Tel.: (34) 96 3543881
58
59
60

1.- Introduction

Silver chromate has been extensively studied at ambient conditions due to its unusual red color, which makes this compound unique as pigment and for colouring applications. Although it remains as a controversial subject, some authors concluded that the intense absorption centred at 450 nm could be explained by a ${}^1T_2 \leftarrow {}^1A_1$ transition of the $[\text{CrO}_4]^{2-}$ anion, red-shifted in the silver salt^{1,2}. Regarding its crystal structure, Ag_2CrO_4 crystallizes in the orthorhombic space group *Pnma* (Nr. 62), with lattice constants: $a = 10.063(11)$ Å, $b = 7.029(4)$ Å, and $c = 5.540(2)$ Å and four formula units per cell ($Z = 4$) at ambient conditions³. The topology of this olivine-like structure is typically described as consisting of isolated chromate $[\text{CrO}_4]$ groups, whose oxygen atoms are coordinated to the silver atoms to generate the tridimensional network (see Fig. 1). Two different types of silver-centred oxygen polyhedra exist: elongated octahedra and distorted off-centered tetrahedra. This crystal structure is also adopted by other ternary oxides such as forsterite Mg_2SiO_4 ⁴, Al_2BeO_4 ⁵ or Ag_2MnO_4 ⁶. The structures of some alkaline-metal chromates like those of potassium⁷, rubidium⁸ and cesium⁹, differ significantly from that of silver chromate even if described in the same space group. Compared to these compounds, the shorter metal-oxygen distances of silver chromate point to a greater degree of covalent bonding between cations and anions¹⁰.

Few experimental studies on Ag_2CrO_4 at high temperature (HT) or high pressure (HP) have been reported¹¹⁻¹⁴. A reversible first-order structural transformation was observed at 490°C by differential thermal analysis, electrical conductivity measurements, and temperature-variable x-ray diffraction^{11,12,14}. The HT phase appears to be hexagonal with $Z=16$ and lattice parameters $a = 9.92(4)$ Å and $c = 19.76(8)$ Å at 506°C¹¹. The phase diagram of silver chromate was studied by Pistorious up to 4 GPa and 900°C and,

1
2
3 besides the aforementioned HT phase, no additional polymorphs were found^{13,14}. With
4
5 regard to polymorphism at extreme conditions, a complementary description of the
6
7 silver chromate structure based on the topology of its cation Ag_2Cr subarray could be
8
9 relevant¹⁵. This cationic framework adopts the Ni_2In structural type, formed by trigonal
10
11 prisms of Ag atoms connected by common edges forming straight chains which run
12
13 parallel to the ab plane (see Fig. 1). Adjacent chains of prisms are shifted $1/2a$ along
14
15 this axis. The Cr atoms ($[\text{CrO}_4]$ groups) are located in the center of such prisms.
16
17 Alkaline-metal chromates of K, Rb, and Cs adopt, however, a Co_2Si -type structure
18
19 which also consists of trigonal prisms of metal atoms but in a zig-zag configuration.
20
21 This alternative view of crystal structures of oxides, together with the well-established
22
23 fact that cations in oxides tend to reproduce the structure of the corresponding or
24
25 intimately-related alloy, could provide a tool to qualitatively predict new pressure-
26
27 induced phases¹⁵. Thus, high-pressure studies on several oxides have shown that high-
28
29 pressure transformations involve an increase of the number of neighbour atoms in their
30
31 second coordination sphere¹⁶⁻¹⁸. Moreover, the behaviour of M_2X compounds (where M
32
33 = group IA or IB elements) under compression¹⁹⁻²⁵ could give some hints of the
34
35 potential transition mechanisms in Ag_2CrO_4 .
36
37
38
39

40
41 Taking this background into account, this work aims at giving a detailed picture of
42
43 the structure and physical properties of silver chromate up to 20 GPa. Angle-dispersive
44
45 x-ray diffraction (ADXRD), Raman spectroscopy, and optical absorption measurements
46
47 suggest that the initial orthorhombic phase undertakes an isostructural transition with a
48
49 drastic volume collapse above 4 GPa and a subsequent transition above 13 GPa.
50
51 Preliminary first-principles calculations are unable to reproduce the isostructural phase
52
53 transition likely due to electronic considerations in chromium atoms.
54
55
56
57
58
59
60

2.- Experimental details

Commercial silver chromate powder with 99.9% purity (Alfa Aesar, Prod. Nr. 7784-01-2) was crushed in a mortar to obtain micron-sized samples. These samples were used to carry out HP-ADXRD, HP-Raman, and HP-optical absorption measurements at room temperature.

2.1.- ADXRD experiments. Three independent HP-ADXRD experiments were conducted in diamond-anvil cells up to 20 GPa. Experiment 1 was carried out using an in-house Xcalibur diffractometer with K_{α} molybdenum radiation (0.7107 Å). The same set-up was previously used to successfully characterize the high-pressure phases of other compounds in the same pressure range²²⁻²⁴. Experiments 2 and 3 were performed at the I15 beamline of Diamond and the MSPD beamline²⁶ of ALBA synchrotron light sources, respectively, with a $40 \times 40 \mu\text{m}$ -focused incident monochromatic beam of 0.4246 Å. The Ag_2CrO_4 metallic-lustered powder samples were loaded in a $150 \mu\text{m}$ -diameter hole of a stainless-steel gasket preindented to a thickness of about $40 \mu\text{m}$. A 16:3:1 methanol:ethanol:water mixture was used as pressure-transmitting medium. Preliminary data reduction was done using the Fit2D software²⁷. Pressure was measured by three different methods: (i) the ruby fluorescence scale²⁸; (ii) the equation of state (EOS) of silver²⁹, which was added as external pressure calibrant in experiments 1 and 2; and (iii) the EOS of copper³⁰ in experiment 3. These methods give a maximum pressure uncertainty of 0.2 GPa at the highest pressure of this study. The observed intensities were integrated as a function of 2θ in order to give one-dimensional diffraction profiles. The indexing and refinement of the powder diffraction patterns were performed using the FULLPROF³¹ and POWDERCELL³² program packages.

1
2
3 **2.2.- Raman experiments.** Unpolarized HP-Raman scattering measurements at room
4 temperature were performed on powder samples in backscattering geometry with a
5 LabRAM HR UV microspectrometer coupled to a Peltier-cooled CCD camera. A
6 632.81 nm (1.96 eV) HeNe laser excitation line with a power around 1 mW and a
7 spectral resolution better than 2 cm^{-1} were used. During Raman experiments, samples
8 were checked by monitoring the time dependence of the Raman signal at different
9 accumulations and by visual inspection before and after each measurement in order to
10 be sure that no heating effects occur during the measurements by the incoming laser
11 excitation since the laser energy was above the band gap energy (1.80 eV). In order to
12 analyze the Raman spectra, Raman peaks have been fitted to a Voigt profile (Lorentzian
13 profile convoluted by a Gaussian profile) where the spectrometer resolution is taken as a
14 fixed Gaussian width (1.5 cm^{-1}). For HP studies the samples were loaded in a
15 membrane-type DAC. A 16:3:1 methanol:ethanol:water mixture was used as pressure-
16 transmitting medium and pressure was measured by the ruby fluorescence scale.²⁸
17
18
19
20
21
22
23
24
25
26
27
28
29
30
31
32
33
34
35

36 **2.3.- Optical absorption measurements.** For optical absorption studies, we used 20-
37 μm -thin platelets cleaved from small single crystals. The single crystals were obtained
38 compressing the Ag_2CrO_4 powder to 1 GPa using a large volume press equipped with
39 Bragg anvils and using hexagonal boron nitride disc as pressure medium and to
40 isolate the sample from the tungsten carbide anvils³³. Measurements in the visible-near-
41 infrared range were done in an optical setup, which consisted of a deuterium lamp,
42 fused silica lenses, reflecting optics objectives, and a visible-near-infrared
43 spectrometer³⁴. For HP-optical absorption studies the samples were loaded in a
44 membrane-type DAC with similar configuration as in HP-ADXRD and HP-Raman
45 experiments. The optical-absorption spectra were obtained from the transmittance
46
47
48
49
50
51
52
53
54
55
56
57
58
59
60

1
2
3 spectra of the sample, which were measured using the sample-in, sample-out
4 method^{35,36}.
5
6
7

8
9 **2.4.- First-principles calculations.** Total-energy *ab initio* simulations have been
10 performed within the density-functional theory (DFT) framework as implemented in the
11 Vienna *ab initio* simulation package (VASP) (see Refs. ³⁷ and ³⁸ and references therein).
12 The program performs *ab initio* structural calculations with the plane-wave pseudo-
13 potential method. The set of plane waves employed extended up to a kinetic energy
14 cutoff of 520 eV. Such a large cutoff was required to achieve highly converged results
15 within the projector-augmented-wave (PAW) scheme ^{38,39}. The PAW method takes into
16 account the full nodal character of the all-electron charge density distribution in the core
17 region. The exchange-correlation energy was taken in the generalized gradient
18 approximation (GGA) with the Perdew-Burke-Ernzerhof (PBE) prescription⁴⁰. It is well
19 known that the GGA approach typically underestimates the cohesion energy ⁴¹ (in turn
20 producing an overestimation of the equilibrium volume). We used dense special point
21 grids appropriate to each structure considered to sample the Brillouin zone (BZ), thus
22 ensuring a high convergence of 1–2 meV per formula unit in the total energy of each
23 structure as well as an accurate calculation of the forces over the atoms. At each
24 selected volume, the structures were fully relaxed to their equilibrium configurations
25 through the calculation of the forces on atoms and the stress tensor⁴¹. In the relaxed
26 equilibrium configuration, the forces were smaller than 0.006 eV/Å, and the deviation
27 of the stress tensor from a diagonal hydrostatic form was less than 0.1 GPa.
28
29
30
31
32
33
34
35
36
37
38
39
40
41
42
43
44
45
46
47
48
49
50

51 Lattice-dynamic calculations of phonon modes were performed at the zone center
52 (□ point) of the BZ. We used a direct force-constant approach (or supercell method)⁴²
53 that it is conceptually simple. These calculations provide information about the
54
55
56
57
58
59
60

1
2
3 symmetry of the modes and their polarization vectors, and allowed us to identify the
4
5 irreducible representations and the character of the phonon modes at the Γ point.
6
7

9 10 **3.- Crystal structure under compression**

11
12 Figures 2 and 3 show the ADXRD data for Ag_2CrO_4 at several selected pressures in
13
14 experiment 3. The other data sets present similar features. At ambient conditions, the X-
15
16 ray diffraction pattern corresponds to the orthorhombic olivine-like structure previously
17
18 reported (S.G. *Pnma*, No. 62) with similar lattice parameters: $a = 10.065(4)$ Å, $b =$
19
20 $7.013(3)$ Å and $c = 5.538(2)$ Å. ADXRD patterns can be indexed in the initial low-
21
22 pressure (LP) orthorhombic phase up to 3.5 GPa. Atomic coordinates do not change
23
24 significantly in this pressure range. For instance, the ADXRD pattern at 2.7 GPa was
25
26 refined by the Rietveld method (see Fig. 2) with an olivine-like model, obtaining the
27
28 final atomic positions collected in Table I. The evolution of the unit-cell volume and
29
30 lattice parameters of this phase are shown in Fig. 4a and 4b, respectively. It can be seen
31
32 that the contraction of the lattice parameters is rather anisotropic. For instance,
33
34 according to our experiments, the relative contractions for a , b , and c between room
35
36 pressure and 3.5 GPa are 1.51, 1.17, and 3.15%, respectively. A third-order Birch-
37
38 Murnaghan EOS gives the following characteristic parameters: (i) a zero-pressure
39
40 volume $V_0 = 391.3(3)$ Å³, (ii) a bulk modulus $B_0 = 52(2)$ GPa, and (iii) its first pressure
41
42 derivative $B'_0 = 5.4(9)$. It is worth to mention that, even considered as an olivine-like
43
44 structure, the different chemical content of Ag_2CrO_4 generates different b/a and c/a axes
45
46 ratios which cause two distinct coordination spheres for the silver atoms (C.N. 6 and 4),
47
48 instead of the quite regular $[\text{MgO}_6]$ octahedra in olivine. This distribution of polyhedra
49
50 and the fact that the Ag – O bonds are significantly more compressible than the Cr – O
51
52 bonds, make compression parallel to the b axis much more restricted than parallel to c .
53
54
55
56
57
58
59
60

1
2
3 Axial compressibility of different olivine-like polymorphs differ considerably due to
4
5 different cation sizes and valences^{5,43}. Resultant bulk moduli also have a huge
6
7 variability, from 242(5) GPa in Al₂BeO₄ chrysoberyl ($B'_0 = 4$, fixed)⁵ to the value
8
9 obtained in this work for Ag₂CrO₄. Note also that the compressibility of K₂CrO₄, with a
10
11 Co₂Si-type cation subarray, is significantly larger ($B_0 = 26(2)$ GPa and $B'_0 = 6.0(5)$)
12
13 than that of Ag₂CrO₄, with a Ni₂In-type cation network⁴⁴.
14
15

16 The LP phase starts to transform into a new HP phase (named HP1) at 3.5 GPa. The
17
18 ADXRD patterns between this pressure and 5 GPa present five new low intense peaks
19
20 below $2\theta = 8.4^\circ$ (synchrotron radiation) and some of the existing Bragg peaks seem to
21
22 slightly broaden. Diffractograms in this pressure range could not be unequivocally
23
24 indexed but the stability of the positions and intensities of most of the peaks suggests
25
26 that only a small distortion of the lattice occurs. Between 5 and 12.5 GPa, the ADXRD
27
28 patterns could be indexed in an orthorhombic cell, whose reflection conditions are
29
30 consistent with a *Pnma* symmetry, similarly to the ambient structure. The formation of
31
32 this new phase entails a volume decrease of 0.95%, mainly caused by the 1.3% collapse
33
34 of the *a* axis (see Fig. 4b). The olivine-like structural model was used as a starting point
35
36 for a Rietveld refinement. The HP1 phase (depicted in Fig. 5) turned out to have the
37
38 same structure that the LP phase. As shown in Table I, the refinement suggests that the
39
40 Ag₂Cr cation subarray seems not to change significantly and only a strong distortion of
41
42 the [CrO₄] tetrahedra is observed, with Cr – O distances at 6.4 GPa ranging from 1.565
43
44 to 1.84 Å (compare to 1.58 – 1.74 Å at 2.7 GPa) and angles ranging from 70 to 132°
45
46 (compare to 104 – 115° at 2.7 GPa). Confirmation of such a strong polyhedral distortion
47
48 by single-crystal HP-ADXRD measurements is advisable. It is worth to mention that the
49
50 coexistence of the LP and HP1 phases would enable explaining two of the extra peaks
51
52 observed between 3.5 and 5 GPa, as well as the apparent broadening of some reflections.
53
54
55
56
57
58
59
60

1
2
3 The zero-pressure volume and the compressibility of the HP1 phase have been
4
5 estimated by fixing the pressure derivative B'_0 to 4: $V_0 = 382(2) \text{ \AA}^3$, $B_0 = 69(3) \text{ GPa}$.
6
7 This phase is a bit less compressible than the initial LP phase, the continuous decrease
8
9 of the lattice parameters being shown in Fig. 4b.
10

11 Above 10 GPa, the diffraction peaks broaden significantly as a consequence of the
12
13 loss of the quasi-hydrostatic conditions and the appearance of deviatoric stresses in the
14
15 compressed sample⁴⁵ (see Fig. 3). These stresses could induce the second high-pressure
16
17 phase (HP2) observed above 13 GPa. The limited quality of the x-ray patterns at these
18
19 pressures avoids unequivocal indexation but the small amount of changes observed at
20
21 the transition suggests either a slow process with coexistence of the HP1 and HP2
22
23 phases during a large pressure range or a low-symmetry distortion of the HP1
24
25 orthorhombic phase. Both high-pressure phase transitions are reversible and the LP
26
27 phase is recovered after decompression with similar lattice constants.
28
29
30
31
32
33

34 4.- Lattice dynamics under compression

35
36 Group theoretical considerations⁴⁶ indicate that the *Pnma* structure of Ag_2CrO_4 has
37
38 36 Raman-active modes with the following mechanical representation $\Gamma = 11A_g + 7B_{1g}$
39
40 $+ 11B_{2g} + 7B_{3g}$, which can be also classified by factor group analysis as internal or
41
42 external modes of the CrO_4 units so that there are 18 internal modes [$2\nu_1, 4\nu_2, 6\nu_3, 6\nu_4$]
43
44 and 18 external modes [6 rotational (R) and 12 translational (T)]¹⁰. Therefore, the 36
45
46 Raman-active modes can be classified as $11A_g (\nu_1, \nu_2, 2\nu_3, 2\nu_4, R, 4T) + 7B_{1g}$
47
48 $(\nu_2, \nu_3, \nu_4, 2R, 2T) + 11B_{2g} (\nu_1, \nu_2, 2\nu_3, 2\nu_4, R, 4T) + 7B_{3g} (\nu_2, \nu_3, \nu_4, 2R, 2T)$. Up to now only 12
49
50 Raman modes were measured for Ag_2CrO_4 at ambient conditions, likely due to
51
52 considerable overlapping of modes¹⁰, while 28 out of 42 Raman modes were measured
53
54
55
56
57
58
59
60

1
2
3 for structurally-related alkaline-earth chromates^{47,48} and 30 out of 36 Raman modes
4
5 have been recently measured in monazite-type PbCrO_4 ⁴⁹.
6

7
8 Figure 6 shows the Raman spectra of Ag_2CrO_4 at room temperature at selected
9
10 pressures till 18.8 GPa. The Raman spectrum of the LP phase is similar to that reported
11
12 earlier¹⁰. The most intense Raman modes are the stretching modes of the CrO_4 group in
13
14 the high-frequency region between 750 and 900 cm^{-1} ^{10,47,48}. Of considerable smaller
15
16 intensity are the bending modes of the CrO_4 group in the medium-frequency region
17
18 between 300 and 400 cm^{-1} . Finally, translational and rotational lattice Raman modes in
19
20 the low-frequency region below 150 cm^{-1} are the most difficult to identify. A change in
21
22 the Raman spectrum can be clearly observed in both the medium- and high-frequency
23
24 regions at 5 GPa. This change is in good agreement with the phase transition suggested
25
26 by ADXRD measurements at similar pressures. A more important change in the Raman
27
28 spectrum is observed above 14.8 GPa; thus confirming the phase transition reported
29
30 around 14 GPa by ADXRD measurements. Raman measurements on downstroke at
31
32 12.8 and 0.1 GPa confirm the reversibility of both phase transitions.
33
34
35

36
37 Figure 7 shows the pressure dependence of the measured Raman mode frequencies
38
39 in Ag_2CrO_4 at room temperature till 19 GPa. Experimental and calculated Raman modes
40
41 for the LP phase are compared till 5 GPa and show a good agreement (see Table II). On
42
43 the other hand, Table III summarizes the frequencies and pressure coefficients of the
44
45 observed Raman modes for the HP1 and HP2 phases at 5 and 14 GPa, respectively. It
46
47 can be observed that the frequencies of the stretching modes above 5 and 14 GPa are
48
49 similar to those of the low-pressure phase, thus suggesting that there is no drastic
50
51 change in coordination during the two phase transitions at least for the Cr atom. In this
52
53 respect, the different pressure dependence of the Raman modes above 14 GPa do not
54
55 suggest the coexistence of HP1 and HP2 phases in a region larger than 1 GPa.
56
57
58
59
60

1
2
3 Furthermore, the larger number of Raman modes observed in the HP2 phase with
4 respect to HP1 suggests that HP2 could be a low-symmetry distortion of the HP1 phase.
5
6
7

9 10 **5.- Optical absorption under compression**

11 Figure 8 shows the optical absorption spectra of Ag_2CrO_4 at room temperature and
12 at selected pressures up to 5.2 GPa. Absorption spectra of the LP phase show a steep
13 absorption, characteristic of a direct bandgap, plus a low-energy absorption band, which
14 overlaps partially with the fundamental absorption. This absorption band has been
15 previously observed in related oxides and seems to be caused by the presence of defects
16 or impurities. Its nature has been the subject of considerable debate and is beyond the
17 scope of this work. Regarding the steep absorption edge, we found it exhibits an
18 exponential dependence on the photon energy following the Urbach's law. Therefore, in
19 order to determine the bandgap energy, E_g , we have analyzed the measured absorption
20 spectrum assuming $\alpha = A_0 \exp[-(E_g - h\nu)/E_u]$. In this equation E_u is Urbach's energy,
21 which is related to the steepness of the absorption tail, and $A_0 = k\sqrt{E_u}$ for a direct band
22 gap, with k being a characteristic parameter. From the analysis of the spectra collected
23 at ambient pressure we determined the bandgap to be 1.8 eV in good agreement with
24 previous studies⁵⁰.
25
26
27
28
29
30
31
32
33
34
35
36
37
38
39
40
41

42 In Fig. 8 it can be seen that upon compression the absorption edge gradually red-
43 shifts up to 4.7 GPa. At 5.2 GPa, an abrupt shift is detected, which produce the color
44 change from brown-red to dark-brown, indicating the occurrence of a bandgap collapse.
45 We associated this change to the first transition detected at similar pressure in
46 diffraction and Raman experiments. At 5.2 GPa, the absorption spectrum also resembles
47 that of a direct bandgap semiconductor. Unfortunately, at higher pressures we could not
48
49
50
51
52
53
54
55
56
57
58
59
60

1
2
3 perform experiments because the sample deteriorates likely due to increasing intergrain
4
5 strains, which prevented the performance of accurate optical measurements.
6

7
8 In order to qualitatively analyze the pressure effects on the bandgap of the LP phase,
9
10 we assumed that the LP and HP1 phases have a fundamental direct bandgap. Using the
11
12 same method employed to determine E_g at ambient conditions, we obtained the pressure
13
14 dependence of E_g . The inset of Figure 8 shows the variation of the E_g versus pressure up
15
16 to 5.2 GPa. The LP phase shows a linear negative pressure coefficient of the bandgap
17
18 energy (-30 meV/GPa) up to the phase transition pressure. From 4.7 to 5.2 GPa, E_g
19
20 abruptly changes from 1.65 to 1.47 eV. Based upon present knowledge of the electronic
21
22 structure of Ag_2CrO_4 at atmospheric pressure and the behavior of other chromates upon
23
24 compression, a qualitative approach toward the understanding of the present results is
25
26 suggested in the following. According to Ouyang et al.⁵⁰, the main contribution to the
27
28 bottom of the conduction band in Ag_2CrO_4 results from the antibonding interaction
29
30 between the Cr 3d orbitals and the Ag 5s5p orbitals, while the upper portion of the
31
32 valence band results primarily from the interaction between Ag 4d and O 2p orbitals.
33
34 Under compression, O 2p states shift toward high energies faster than the Cr 3d states
35
36 because of the increase of the crystal field. This causes a reduction of the energy
37
38 difference between the bottom of the conduction band and the top of the valence band,
39
40 inducing the E_g reduction we observed up to 4.7 GPa. On the other hand, the collapse of
41
42 E_g observed at 5.2 GPa could be caused by the structural change we found at similar
43
44 pressures. Although the structural changes do not affect the global symmetry of the
45
46 crystal, the crystal structure is highly distorted, affecting Cr-O and Ag-O bond angles
47
48 and distances. These changes of the crystalline structure should be directly reflected in
49
50 the electronic structure of Ag_2CrO_4 , producing the collapse of E_g that we observed.
51
52
53
54
55
56
57
58
59
60

6.- First-principles calculations under compression

Total-energy (E) calculations as a function of volume were performed for five different high-pressure structural candidates of Ag_2CrO_4 . The choice of these potential phases is justified by: (i) the expected analogy with the pressure-induced sequence in M_2X compounds (thenardite (Na_2SO_4 -type, $Fddd$) and spinel (Na_2MoO_4 -type, $Fd-3m$)), (ii) the expected analogy with pressure-induced transformations in olivine (wadsleyite ($Imma$), spinel) or (iii) possible structural similarities with chemically-related compounds ($Pnma$ K_2CrO_4 -type or $Pbnn$ Na_2CrO_4 -type).

After performing a full optimization of the lattice parameters and atomic positions, we found that, as expected, the initial $Pnma$ phase is the structure of Ag_2CrO_4 with the lowest enthalpy at ambient pressure. A fit with a Birch-Murnaghan third-order equation of state (EOS) gives the following characteristic parameters in good agreement with experimental results: $V_0 = 408.2 \text{ \AA}^3$, $B_0 = 50.2 \text{ GPa}$ and $B'_0 = 5.7$ (see also Fig. 4). The equilibrium volume V_0 is overestimated by $\sim 4 \%$, as usual with the GGA approximation. Our first-principles calculations using the GGA approximation do not predict any volume collapse in the initial $Pnma$ structure at high pressures. The addition of the on-site repulsion Hubbard term U to Ag and Cr atoms did not help either to reproduce the structural behavior of the orthorhombic Ag_2CrO_4 phase. Therefore, these experimental and theoretical evidences seem to indicate that a new structural and electronic description is required to model the properties of silver chromate. Low-symmetry subgroups of the initial Ag_2CrO_4 phase (space group Nrs. 31, 26, 19, 14 and 11) were also considered as HP candidates but, after relaxation of the lattice parameters and the atomic coordinates, all of them could be described within a $Pnma$ space group.

Only the spinel-type structure has been found to be energetically competitive at high pressures for silver chromate (see Figure 9). The spinel-type structure, with cubic

1
2
3 symmetry, becomes more stable than the *Pnma* phase at a pressure of 11 GPa, after a
4 first order phase transition with 2.7% decrease in the volume. The spinel phase,
5 however, has not been found experimentally in the pressure range covered in our
6 experiments. This may be caused by the presence of kinetic-energy barriers or
7 temperature effects that avoid the transformation.
8
9
10
11
12

13 14 15 16 **7.- Concluding remarks**

17
18 Three different characterization techniques, i.e. X-ray diffraction, optical absorption
19 and Raman spectroscopy, evidence the existence of two pressure-induced phase
20 transitions in silver chromate, at 4 and 13 GPa. The first HP phase could be indexed into
21 an orthorhombic cell similar to that adopted at ambient pressure, and the atomic
22 coordinates of Ag and Cr atoms did not change significantly. Only a considerable
23 distortion of the [CrO₄] seems to take place but the structure can still be described
24 within the initial *Pnma* space group. Consequently, the transition can be considered as
25 an isostructural transition. This collapse is mainly due to the drastic contraction of the *a*
26 axis (~1.3%). We note that a similar rare transition was also recently observed in other
27 chromate, the cubic perovskite PbCrO₃, which suffers a large volume collapse in an
28 isostructural transition⁵¹.
29
30
31
32
33
34
35
36
37
38
39
40
41
42

43 A second phase transition occurs at ~13 GPa, to an unknown structure which,
44 Raman and x-ray diffraction data suggests could be a low-symmetry intimately-related
45 polymorph. First-principles calculations have been unable to reproduce both phase
46 transitions likely due to electronic considerations in Ag and Cr atoms and, in the case of
47 the second transition, to the existence of non-hydrostatic conditions in the experiment.
48 Instead, they predict a high pressure transformation to the spinel structure at 11 GPa,
49
50
51
52
53
54
55
56
57
58
59
60

1
2
3 which experimentally was not observed in the studied pressure range likely due to the
4
5 existence of kinetic effects
6
7
8

9 10 **8.- Acknowledgements**

11 This study was supported by the Spanish government MEC under Grants No:
12
13 MAT2010-21270-C04-01/03/04 and CTQ2009-14596-C02-01, by the Comunidad de
14
15 Madrid and European Social Fund (S2009/PPQ-1551 4161893), by MALTA Consolider
16
17 Ingenio 2010 project (CSD2007-00045), and by the Vicerrectorado de Investigación y
18
19 Desarrollo of the Universidad Politécnica de Valencia (UPV2011-0914 PAID-05-11
20
21 and UPV2011-0966 PAID-06-11). A.M. and P.R-H. acknowledge computing time
22
23 provided by Red Española de Supercomputación (RES) and MALTA-Cluster. Diamond
24
25 and ALBA Synchrotron Light Sources are acknowledged for provision of beamtime.
26
27 We also wish to thank Drs. Peral, Popescu and Fauth for technical support.
28
29
30
31
32
33

34 **9.- References**

- 35 1. Robbins, D. J.; Day, P. *Molec. Phys.* **1977**, *34*, 893.
- 36 2. Clark, R. J. H.; Dines, T. J. *Inorg. Chem.* **1982**, *21*, 3585.
- 37 3. Hackert, M. L.; Jacobson, R. A. *J. Solid State Chem.* **1971**, *3*, 364.
- 38 4. Birle, J. D.; Gibbs, G. V.; Moore, P. B.; Smith, J. V. *Amer. Miner.* **1968**, *53*, 807.
- 39 5. Hazen, R. M. *Phys. Chem. Miner.* **1987**, *14*, 13.
- 40 6. Chang, F. M.; Jansen, M. Z. *Anorg. Allg. Chem.* **1983**, *507*, 59.
- 41 7. Zachariasen, W. H.; Ziegler, G. E. *Z. Kristallogr.* **1931**, *80*, 164.
- 42 8. Smith, H. W.; Colby, M. Y. *Z. Kristallogr.* **1941**, *103*, 90.
- 43 9. Miller, J. J. *Z. Kristallogr.* **1938**, *99*, 32.
- 44 10. Carter, R. L. *Spectr. Lett.* **1972**, *5*, 401.
- 45 11. Natarajan, M.; Secco, E. A. *Can. J. Chem.* **1974**, *52*, 712.
- 46 12. Cieslak-Golonka, M. *J. Thermal Anal.* **1992**, *38*, 2501.
- 47 13. Pistorius, C. W. F. T.; Boeyens, J. C. A. *Z. Kristallogr.* **1970**, *372*, 263.
- 48 14. Pistorius, C. W. F. T. *J. Chem. Phys.* **1967**, *46*, 2167.
- 49
50
51
52
53
54
55
56
57
58
59
60

- 1
 - 2
 - 3
 - 4
 - 5
 - 6
 - 7
 - 8
 - 9
 - 10
 - 11
 - 12
 - 13
 - 14
 - 15
 - 16
 - 17
 - 18
 - 19
 - 20
 - 21
 - 22
 - 23
 - 24
 - 25
 - 26
 - 27
 - 28
 - 29
 - 30
 - 31
 - 32
 - 33
 - 34
 - 35
 - 36
 - 37
 - 38
 - 39
 - 40
 - 41
 - 42
 - 43
 - 44
 - 45
 - 46
 - 47
 - 48
 - 49
 - 50
 - 51
 - 52
 - 53
 - 54
 - 55
 - 56
 - 57
 - 58
 - 59
 - 60
15. Vegas, A.; Jansen, M. *Acta Cryst. B* **2002**, *58*, 38.
16. Santamaria-Perez, D.; Gracia, L.; Garbarino, G.; Beltran, A.; Chulia-Jordan, R.; Gomis, O.; Errandonea, D.; Ferrer-Roca, C.; Martinez-Garcia, D.; Segura, A. *Phys. Rev. B* **2011**, *84*, 054102.
17. Santamaria-Perez, D.; Chulia-Jordan, R. *High Press. Res.* **2012**, *32*, 81.
18. Santamaria-Perez, D.; Kumar, R. S.; Dos Santos-Garcia, A. J.; Errandonea, D.; Chulia-Jordan, R.; Saez-Puche, R.; Rodriguez-Hernandez, P.; Muñoz, A. *Phys. Rev. B* **2012**, *86*, 094116.
19. Grzechnik, A.; Vegas, A.; Syassen, K.; Loa, I.; Hanfland, M.; Jansen, M. *Journal of Solid State Chemistry* **2000**, *154*, 603.
20. Vegas, A.; Grzechnik, A.; Syassen, K.; Loa, I.; Hanfland, M.; Jansen, M. *Acta Crystallogr. Sect. B-Struct. Sci.* **2001**, *57*, 151.
21. Vegas, A.; Grzechnik, A.; Hanfland, M.; Muhle, C.; Jansen, M. *Solid State Sci.* **2002**, *4*, 1077.
22. Santamaria-Perez, D.; Vegas, A.; Muehle, C.; Jansen, M. *Acta Crystallogr. B, Struct. Sci.* **2011**, *B67*, 109.
23. Santamaria-Perez, D.; Vegas, A.; Muehle, C.; Jansen, M. *Journal of Chemical Physics* **2011**, *135*, 054511.
24. Santamaria-Perez, D.; Marques, M.; Chulia-Jordan, R.; Menendez, J. M.; Gomis, O.; Ruiz-Fuertes, J.; Sans, J. A.; Errandonea, D.; Recio, J. M. *Inorganic Chemistry* **2012**, *51*, 5289.
25. Santamaria-Perez, D.; Morales-Garcia, A.; Martinez-Garcia, D.; Garcia-Domene, B.; Muhle, C.; Jansen, M. *Inorg. Chem.* **2012**, In Press.
26. Knapp, M.; Peral, I.; Nikitina, M.; Quispe, M.; Ferrer, S. *Z. Kristallogr. Proc.* **2011**, *1*, 137.
27. Hammersley, A. P.; Svensson, S. O.; Hanfland, M.; Fitch, A. N.; Hausermann, D. *High Pressure Res.* **1996**, *14*, 235.
28. Mao, H. K.; Xu, J.; Bell, P. M. *Journal of Geophysical Research-Solid Earth and Planets* **1986**, *91*, 4673.
29. Akahama, Y.; Kawamura, H.; Singh, A. K. *J. Appl. Phys.* **2004**, *95*, 4767.
30. Dewaele, A.; Loubeyre, P.; Mezouar, M. *Phys. Rev. B* **2004**, *70*, 094112.
31. Rodriguez-Carvajal, J. *Physica B* **1993**, *192*, 55.
32. Nolze, G.; Kraus, W. *Powder Diffr.* **1998**, *13*, 256.
33. Errandonea, D. *J. Appl. Phys.* **2010**, *108*, 033517.

- 1
2
3
4
5
6
7
8
9
10
11
12
13
14
15
16
17
18
19
20
21
22
23
24
25
26
27
28
29
30
31
32
33
34
35
36
37
38
39
40
41
42
43
44
45
46
47
48
49
50
51
52
53
54
55
56
57
58
59
60
34. Lacomba-Perales, R.; Errandonea, D.; Segura, A.; Ruiz-Fuertes, J.; Rodriguez-Hernandez, P.; Radescu, S.; Lopez-Solano, J.; Mujica, A.; Muñoz, A. *J. Appl. Phys.* **2011**, *110*, 043703.
35. Panchal, V.; Errandonea, D.; Segura, A.; Rodriguez-Hernandez, P.; Muñoz, A.; Lopez-Moreno, S.; Bettinelli, M. *J. Appl. Phys.* **2011**, *110*, 043723.
36. Errandonea, D.; Martinez-Garcia, D.; Lacomba-Perales, R.; Ruiz-Fuertes, J.; Segura, A. *Appl. Phys. Lett.* **2006**, *89*, 091913.
37. Kresse, G.; Furthmuller, J. *Phys. Rev. B* **1996**, *54*, 11169.
38. Kresse, G.; Joubert, D. *Phys. Rev. B* **1999**, *59*, 1758.
39. Blochl, P. E. *Phys. Rev. B* **1994**, *50*, 17953.
40. Perdew, J. P.; Burke, K.; Ernzerhof, M. *Phys. Rev. Lett.* **1996**, *77*, 3865.
41. Mujica, A.; Rubio, A.; Muñoz, A. *Rev. Mod. Phys.* **2003**, *75*, 863.
42. Parlinski, K.; Li, Z.Q.; Kawazoe, Y. *Phys. Rev. Lett.* **1997**, *78*, 4063.
43. Zhang, L. *Phys. Chem. Miner.* **1998**, *25*, 308.
44. Edwards, C. M.; Haines, J.; Butler, I. S.; Leger, J.-M. *J. Phys. Chem. Solids* **1999**, *60*, 529.
45. Klotz, S.; Chervin, J. C.; Munsch, P.; Le Marchand, G. *J. Phys. D: Appl. Phys.* **2009**, *42*, 075413.
46. Kroumova, E.; Arroyo, M. I.; Perez-Mato, J. M.; Kirov, A.; Capillas, C.; Ivantchev, S.; Wondratschek, H. *Phase Transitions* **2003**, *76*, 155.
47. Carter, R. L.; Bricker, C. E. *Spectr. Acta.* **1971**, *27A*, 569.
48. Serghiou, G.; Guillaume, C. *J. Solid State Chem.* **2004**, *177*, 4672.
49. Bandiello, E.; Errandonea, D.; Martinez-Garcia, D.; Santamaria-Perez, D.; Manjon, F. J. *Phys. Rev. B* **2012**, *85*, 024108.
50. Ouyang, S. X.; Li, Z. S.; Ouyang, Z.; Yu, T.; Ye, J. H.; Zou, Z. G. *J. Phys. Chem. C* **2008**, *112*, 3134.
51. Xiao, W.; Tan, D.; Xiong, X.; Liu, J.; Xu, J. *Proc. Nat. Acad. Sci.* **2010**, *107*, 14026.

Table I.- Lattice parameters and Rietveld-refined fractional coordinates for the LP phase at ambient pressure and 2.7 GPa, and for the HP1 phase at 6.4 GPa.

	RP experiment	RP theory	2.7 GPa	6.4 GPa
a axis (Å)	10.065(4)	10.224	9.953(2)	9.682(3)
b axis (Å)	7.013(3)	7.025	6.9570(14)	6.862(2)
c axis (Å)	5.538(2)	5.653	5.4078(8)	5.3349(9)
Unit cell volume (Å³)	390.9(4)	406.02	374.5(2)	354.4(3)
x_{Ag2}	0.1357(8)	0.1412	0.1364(9)	0.146(3)
z_{Ag2}	0.4916(14)	0.4827	0.5115(19)	0.522(3)
x_{Cr}	0.312(2)	0.3182	0.3130(19)	0.316(5)
z_{Cr}	1.003(3)	0.9633	0.983(5)	1.012(7)
x_{O1}	0.148(5)	0.1553	0.137(6)	0.149(19)
z_{O1}	0.919(8)	0.9051	0.974(13)	1.026(24)
x_{O2}	0.356(6)	0.3466	0.351(7)	0.389(11)
z_{O2}	0.265(9)	0.2558	0.270(12)	0.275(3)
x_{O3}	0.386(3)	0.3865	0.382(5)	0.441(7)
y_{O3}	0.442(4)	0.4429	0.454(5)	0.402(7)
z_{O3}	0.876(5)	0.8439	0.873(6)	0.940(9)

Table II.- Symmetries, zero-pressure frequencies, and pressure coefficients of the theoretical and experimental Raman-active modes of the LP phase of Ag_2CrO_4 .

	ω_0 (th.) (cm^{-1})	a (th.) ($\text{cm}^{-1}/\text{GPa}$)	ω_0 (exp.) (cm^{-1})	a (exp.) ($\text{cm}^{-1}/\text{GPa}$)		ω_0 (th.) (cm^{-1})	a (th.) ($\text{cm}^{-1}/\text{GPa}$)	ω_0 (exp.) (cm^{-1})	a (exp.) ($\text{cm}^{-1}/\text{GPa}$)
B_{3g}	13.1(1)	0.7(1)			B_{1g}	320.8(3)	2.7(1)		
A_g	36.3(1)	1.0(1)			B_{3g}	321.0(2)	1.8(1)		
B_{1g}	40.4(3)	-1.3(2)			A_g	328.3(6)	0.6(2)		
B_{2g}	45.6(3)	1.1(1)			B_{2g}	330.0(3)	-0.9(1)		
A_g	51.2(1)	1.8(1)			B_{2g}	335.6(1)	1.9(1)	338(2)	1.4(2)
B_{2g}	61.0(1)	1.3(1)			B_{1g}	342.0(6)	1.2(2)		
B_{3g}	92.2(2)	4.7(1)			A_g	351.9(1)	0.13(4)		
A_g	104.6(7)	4.5(1)			B_{3g}	354.9(5)	1.5(1)	353(2)	2.9(3)
A_g	112.0(3)	4.8(1)	116(1)	2.6(1)	A_g	361.1(2)	2.4(1)	373(1)	2.7(2)
B_{2g}	117.6(5)	4.4(2)			B_{2g}	384.4(1)	2.1(1)		
B_{1g}	129.5(1)	2.9(1)			A_g	769.4(6)	3.3(2)	776(1)	5.5(2)
B_{2g}	139.4(5)	3.7(2)			B_{2g}	778.5(5)	1.4(2)		
B_{3g}	143.5(6)	3.7(2)			A_g	810.4(3)	1.7(1)	812(1)	0.9(1)
B_{2g}	148.8(2)	4.2(1)			A_g	830.0(3)	1.5(1)	826(2)	1.5(1)
B_{1g}	161.0(6)	6.4(2)			B_{3g}	839.6(5)	4.4(2)		
A_g	161.8(2)	3.7(1)			A_g	847.1(5)	4.3(2)	849(3)	3.8(2)
B_{1g}	216.6(3)	4.7(1)			B_{2g}	849.2(8)	-0.1(1)		
B_{3g}	225.5(4)	5.5(1)			B_{2g}	858.3(2)	2.4(2)	859(3)	2.6(1)

Table III.- Frequencies and pressure coefficients of the experimental Raman-active modes of the HP1 and HP2 phases of Ag_2CrO_4 at 5 and 14 GPa, respectively, after fit to equation $\omega=\omega_0+a*P$.

Phase II (5 GPa)			Phase III (14 GPa)		
Mode	ω_0 (exp.) (cm^{-1})	a (exp.) ($\text{cm}^{-1}/\text{GPa}$)	Mode	ω_0 (exp.) (cm^{-1})	a (exp.) ($\text{cm}^{-1}/\text{GPa}$)
1	73(2)	0.8(1)	1	131(1)	0.8(1)
2	92(2)	0.8(1)	2	170(1)	-0.03(1)
3	119(2)	1.5(1)	3	214(1)	-0.9(1)
4	239(3)	4.4(2)	4	216(1)	1.6(1)
5	316(2)	-0.5(1)	5	243(1)	2.1(1)
6	345(2)	0.3(1)	6	351(2)	-3.9(1)
7	379(2)	2.1(2)	7	368(2)	-0.08(1)
8	808(1)	0.9(1)	8	385(2)	2.5(1)
9	823(1)	2.9(1)	9	415(9)	3.6(5)
10	853(1)	1.6(2)	10	816(1)	-1.0(1)
			11	819(1)	1.1(1)
			12	831(2)	1.6(1)
			13	852(2)	1.1(2)
			14	859(3)	4.7(2)

Table IV.- Lattice parameters and fractional coordinates for the spinel-type phase at 14.4 GPa, predicted from first-principles calculations above 11 GPa: S.G. Fd-3m (Nr. 227), origin choice 2.

Lattice parameter: $a = 8.759 \text{ \AA}$				
Unit cell volume: $V = 672 \text{ \AA}^3$				
Atom	Wyckoff position	x	y	z
Ag	16c	0	0	0
Cr	8b	0.375	0.375	0.375
O	32e	0.26508	0.26508	0.26508

Figure captions

Figure 1.- (Color online) Projection along the *c* axis of the low-pressure olivine-like *Pnma* phase of silver chromate. Coordination polyhedra around the Ag and Cr atoms are depicted in gray and yellow, respectively.

Figure 2.- (Color online) X-ray powder diffraction patterns of Ag_2CrO_4 at three selected pressures below 10 GPa. The calculated profiles and the residuals of the Rietveld refinements at 2.7 and 6.4 GPa are represented as red and blue lines, respectively. Vertical marks indicate the Bragg reflections of the orthorhombic *Pnma* Ag_2CrO_4 structure and metallic copper, which was used as a second internal pressure calibrant. The asterisk marks the appearance of the most intense diffraction peak of the gasket.

Figure 3.- X-ray powder diffraction patterns of Ag_2CrO_4 at three selected pressures above 10 GPa. Vertical marks indicate the Bragg reflections of the orthorhombic *Pnma* Ag_2CrO_4 structure and metallic copper at 11.4 GPa.

Figure 4.- (Color online) Evolution of the volume (a) and the lattice parameters (b) of the low-pressure and the HP1 phases of Ag_2CrO_4 with pressure. Red, black and green symbols correspond to XRD data according to Xcalibur, Diamond and ALBA experiments. In (b), the *a*/2, *b*, and *c* axes are represented by squares, circles, and triangles, respectively. Dashed and solid lines correspond to fittings to our experimental data and results from theoretical calculations.

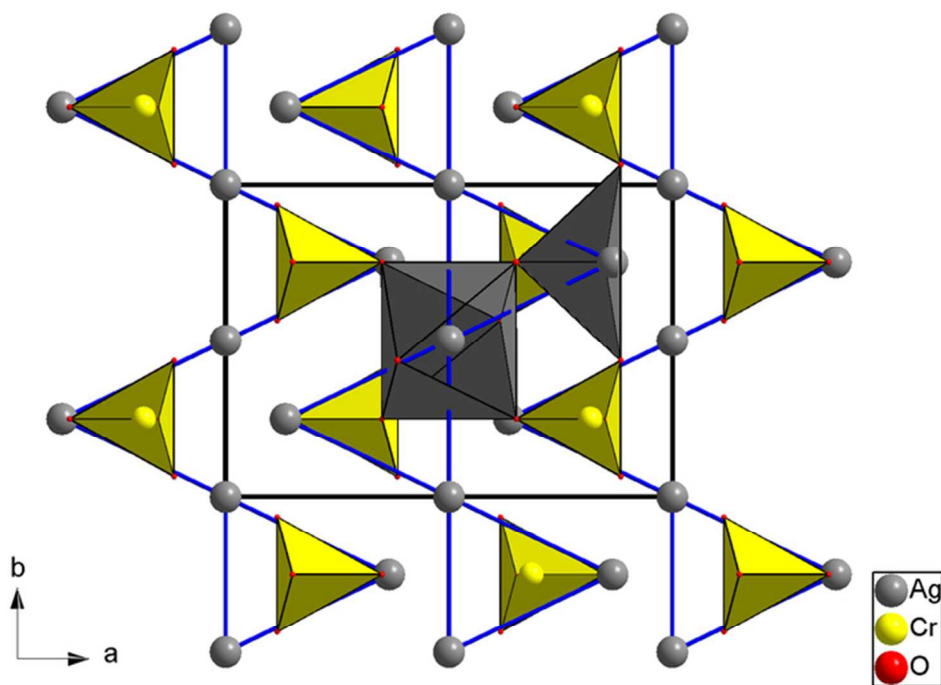
Figure 5.- (Color online) Projection along the *c* axis of the HP1 *Pnma* phase of silver chromate, to be compared to Fig. 1. As can be seen the cation Ag_2Cr subarray still adopts a Ni_2In -type structure, but the Ag and Cr coordination polyhedra are rather distorted.

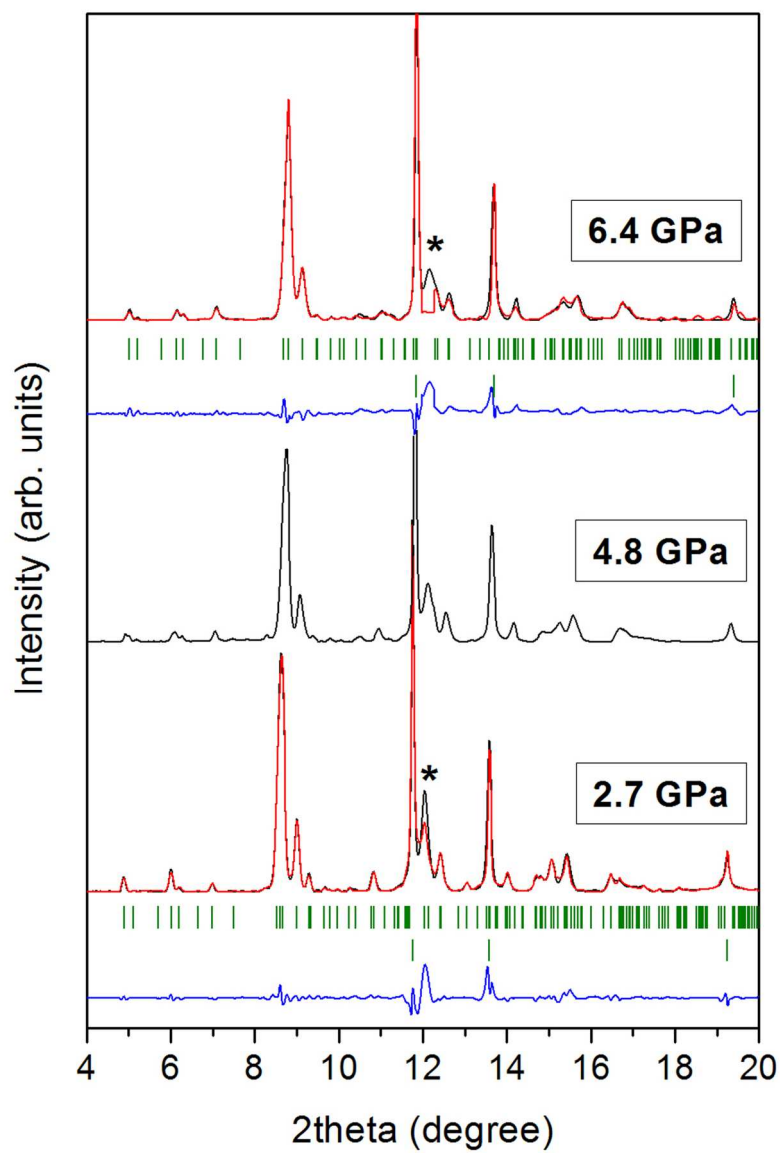
Figure 6.- Raman scattering spectra of Ag_2CrO_4 at selected pressures till 18.8 GPa on upstroke and down to ambient pressure on downstroke (d). Two reversible phase transitions around 5 and 14 GPa have been observed.

1
2
3
4
5 **Figure 7.-** (Color online) Pressure dependence of the Raman-active modes in Ag_2CrO_4 .
6 Red, blue, black, and pink black circles (experimental) and lines (theoretical) refer to A_g ,
7 B_{1g} , B_{2g} , and B_{3g} modes of the low-pressure phase, respectively. Raman-active modes of
8 the HP1 and HP2 high-pressure phases above 5 and 14 GPa are noted with triangles and
9 squares, respectively.
10
11
12

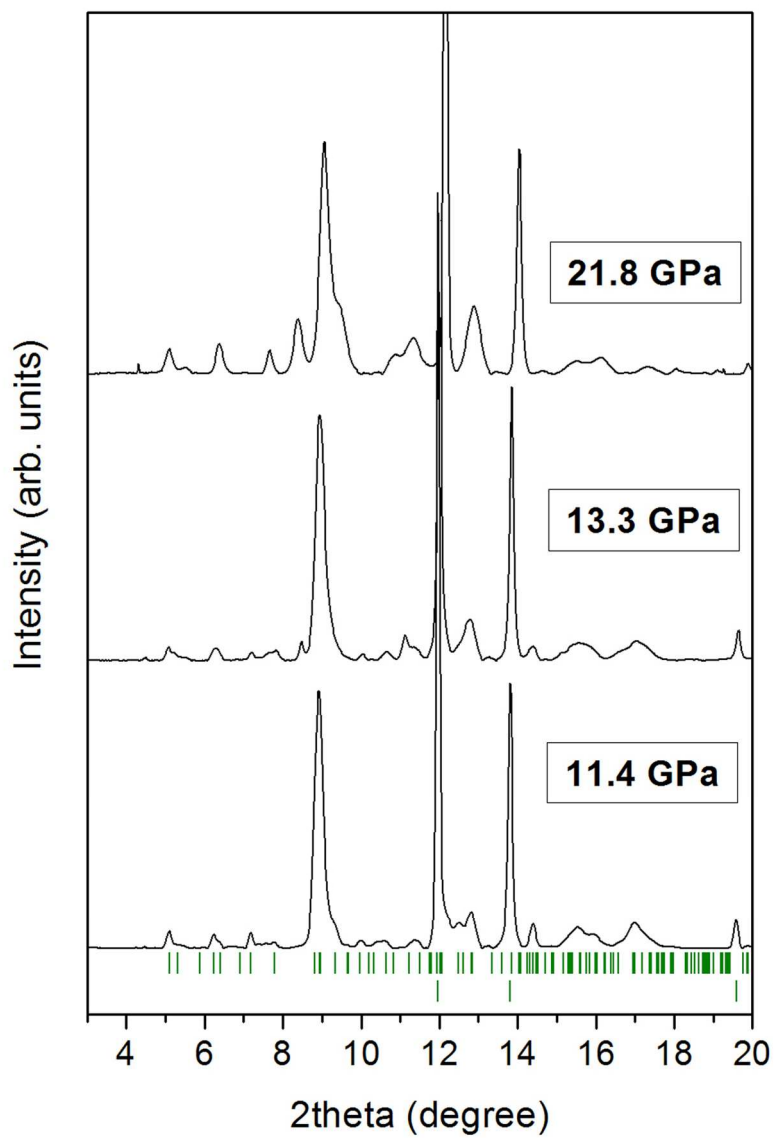
13
14 **Figure 8.-** Optical absorption spectrum of Ag_2CrO_4 at selected pressures till 5.2 GPa.
15 Inset shows the pressure dependence of the bandgap energy.
16
17
18

19 **Figure 9.-** Energy as a function of volume curves for the initial $Pnma$ phase and the
20 spinel-type phase. Both curves cross each other at a volume corresponding to a pressure
21 of 11 GPa. Energy and volume are written per formula unit.
22
23
24
25
26
27
28
29
30
31
32
33
34
35
36
37
38
39
40
41
42
43
44
45
46
47
48
49
50
51
52
53
54
55
56
57
58
59
60

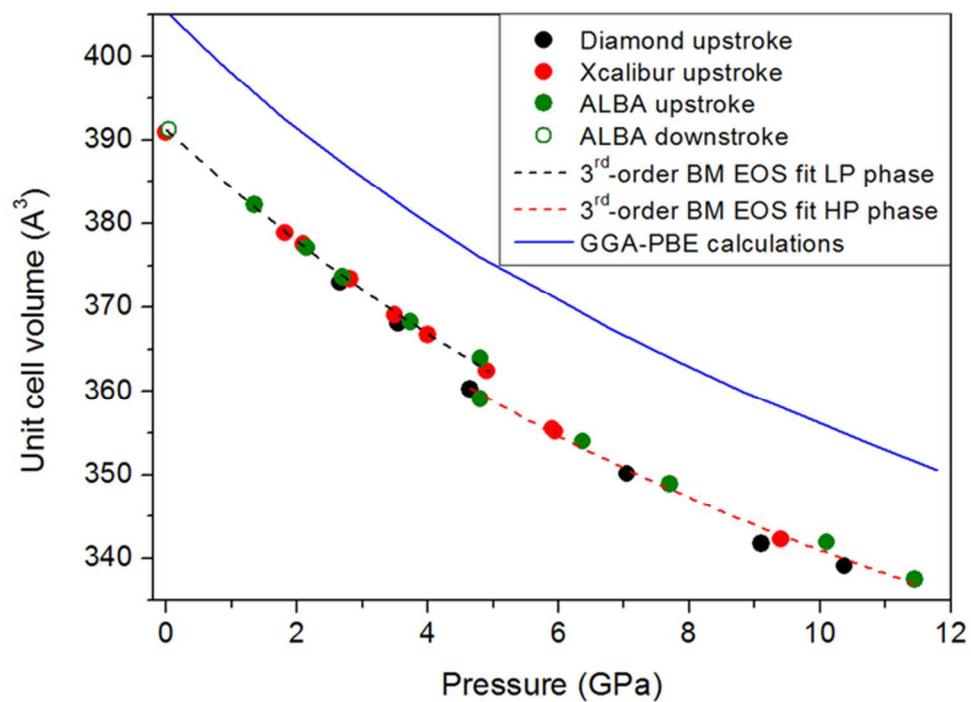




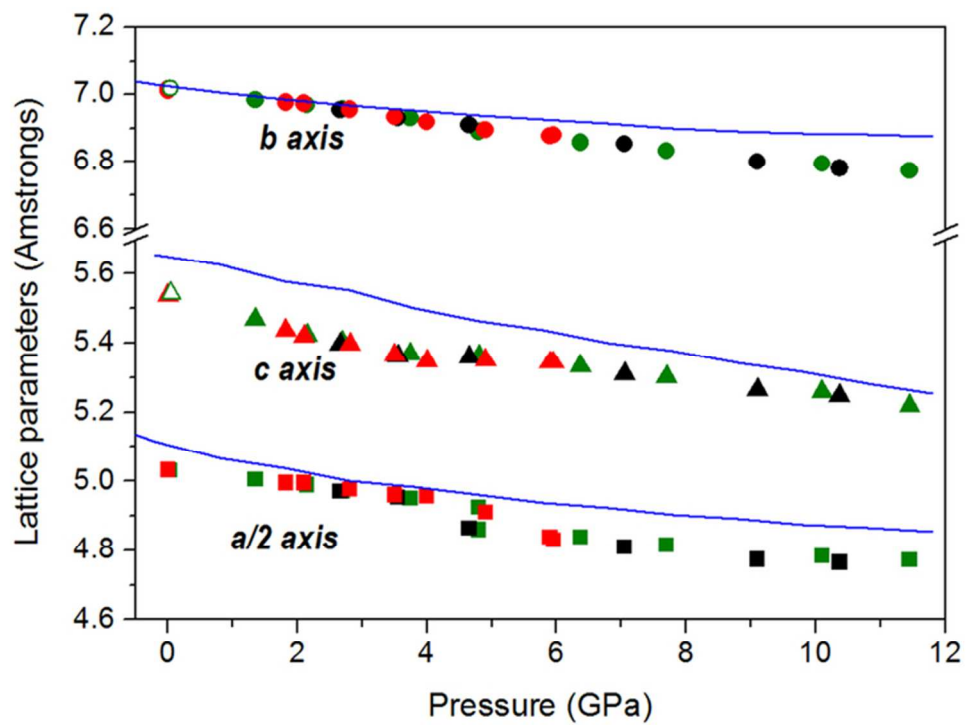
122x178mm (300 x 300 DPI)



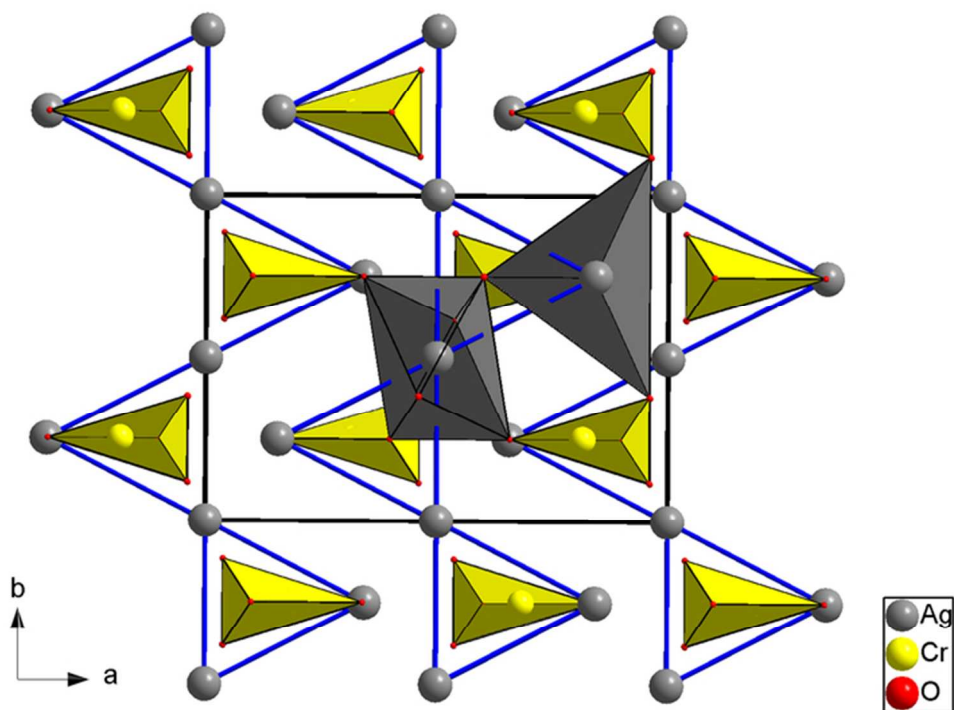
123x181mm (300 x 300 DPI)

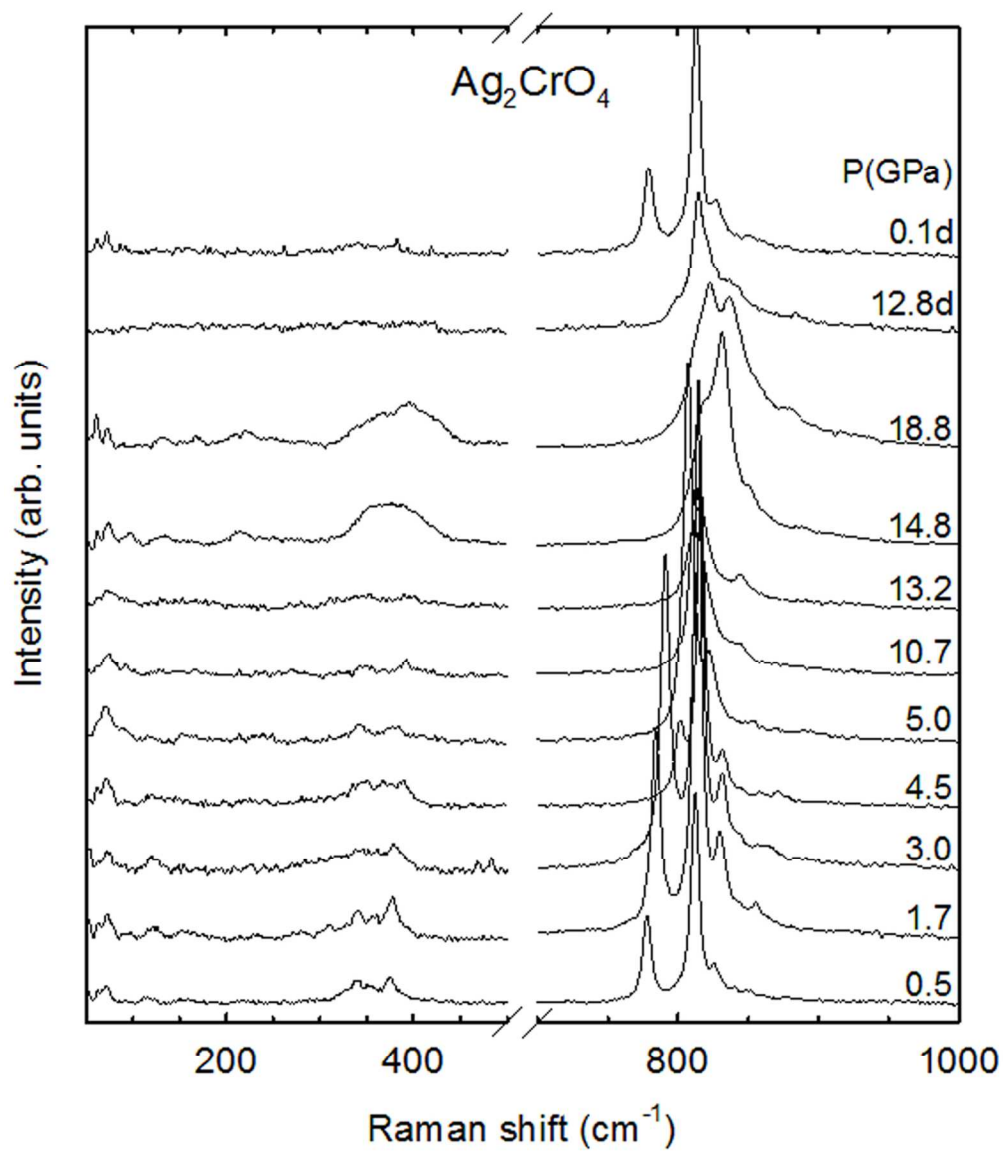


62x45mm (300 x 300 DPI)

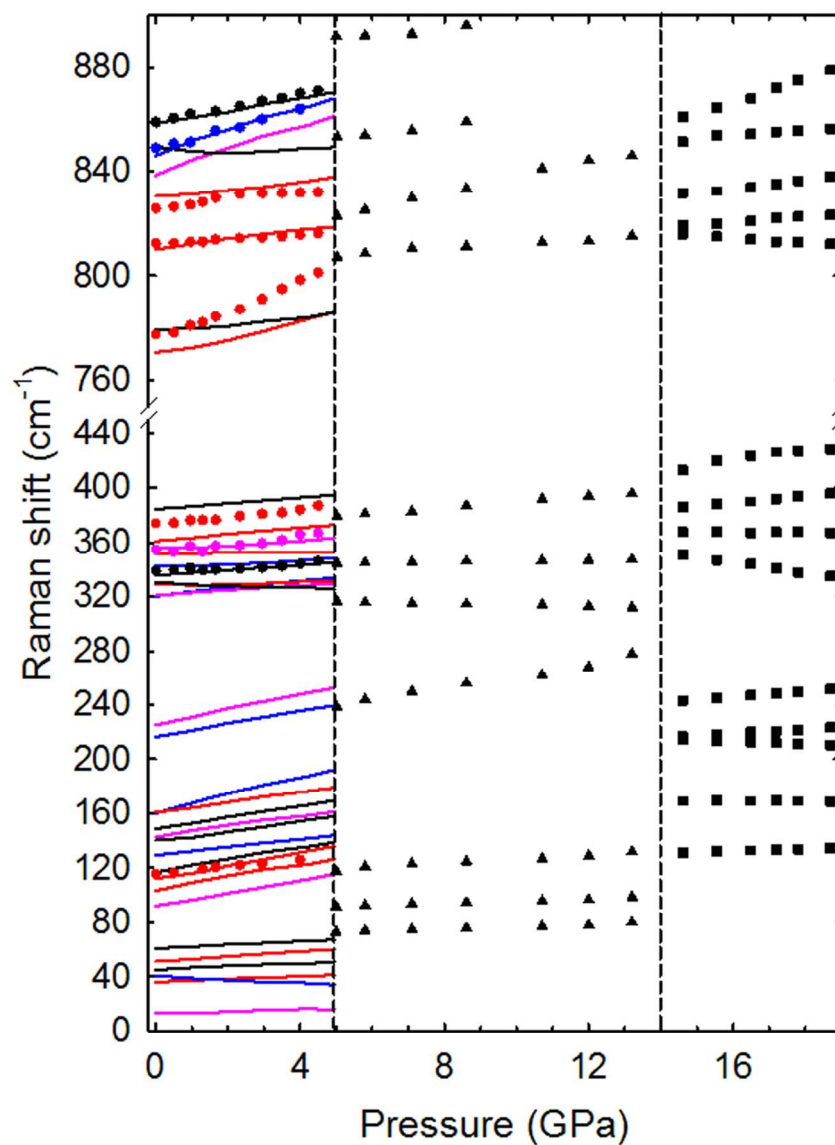


63x48mm (300 x 300 DPI)

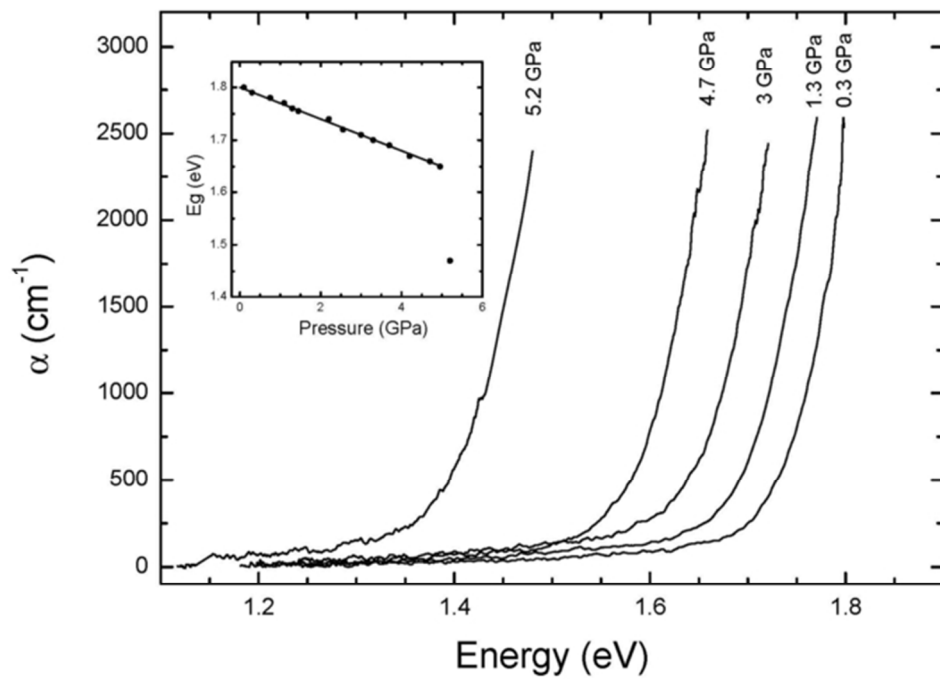




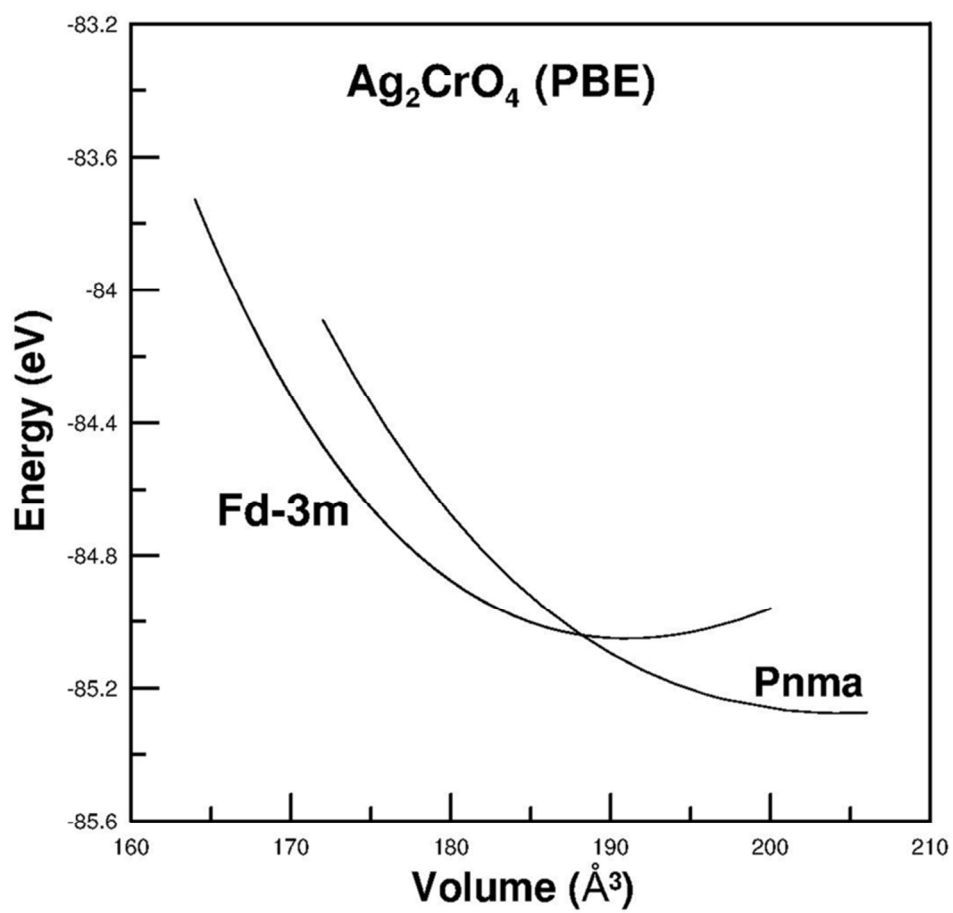
99x117mm (300 x 300 DPI)



115x159mm (300 x 300 DPI)



60x43mm (300 x 300 DPI)



80x77mm (300 x 300 DPI)